Novel Limits on Dark Photon Mixing from Radiation Safety

Wen Yin
Department of Physics, Tokyo Metropolitan University, Minami-Osawa, Hachioji-shi, Tokyo 192-0397, Japan

(Received 26 August 2025; revised 26 October 2025; accepted 16 March 2026; published 3 April 2026)

I propose a novel laboratory search for dark photons based on radiation-safety monitoring at synchrotron radiation facilities, including NanoTerasu, SPring-8, the KEK Photon Factory, and the European Synchrotron Radiation Facility. Dark photons can be produced parasitically in undulators or via photon-mirror interactions and subsequently traverse optical systems and shielding. Taking into account quantum effects and the internal structure of undulators, mirrors, and detectors, I show that even a simple Geiger-Müller counter routinely used for radiation-safety monitoring can detect such dark photons outside the shielding and set the strongest purely laboratory limits on the kinetic mixing parameter, $\chi \lesssim 5 \times 10^{-6}$, in the mass range 1–50 eV. Since radiation safety is strictly regulated, the resulting limits provide robust and realistic constraints.

DOI: 10.1103/snnn-wqxg

Introduction—The search for light and weakly interacting particles, such as axionlike particles (ALPs) and dark photons, has attracted significant attention since they provide simple extensions of the standard model and can explain various aspects such as dark matter, inflation, and the smallness of the nucleon electric dipole moment. There are two broad approaches to searching for such particles: one may attempt to detect them as they are produced in nature—for instance, from astrophysical or cosmological sources—or to generate and detect them under controlled laboratory conditions. The latter approach offers the advantage that systematic uncertainties can be more reliably understood and managed, thereby allowing for more robust searches, although the sensitivity is usually lower compared to astrophysical observations.

Among laboratory searches, light-shining-through-a-wall (LSW) experiments represent a well-established and versatile method [1–11]. In these setups, an intense photon beam is directed at an opaque barrier, and hypothetical particles such as ALPs or dark photons may be produced through photon-new particle conversion. These particles, unlike photons, can traverse the barrier and subsequently reconvert into photons that can be detected. Dedicated LSW experiments have been implemented at laser facilities and synchrotron light sources.

Recently, it has been proposed by the present author and Yoshida in [12] that synchrotron radiation facilities, such as NanoTerasu, SPring-8, the KEK Photon Factory (PF), and the European Synchrotron Radiation Facility (ESRF), allow for a novel "parasitic" LSW-type search. The key idea is that ALPs or dark photons may already be generated in the undulators of the light source. Thus, by placing a detector outside the shielding along the beam line, one can exploit the intense synchrotron photon flux without interfering with the primary operation of the facility. Indeed, such positions usually exist. In [13], the dark photon system for the parasitic LSW is carefully studied by taking into account the momentum integration within the wave packet, the attenuation of photons in a lead wall, and the suppression of mixing due to the medium effects. There, the detector is assumed to be an ideal one. It was shown that, depending on the mass range, the conversion rate can differ significantly from the naïve application of the well-known photon-dark-photon oscillation formula.

In this Letter, I study a more realistic setup inspired by various synchrotron facility designs, and provide a detailed investigation of a simple and well-known detector: the Geiger-Müller (GM) counter. In particular, I demonstrate that even with such a basic radiation monitor—specifically, a GM counter that can serve as an efficient detector for x-ray dark photons—one can already place competitive bounds on dark photons with mass 1–50 eV [14].

The experimental setup is shown in the left panel of Fig. 1. Before going into the details, let me provide an order-of-magnitude estimate to illustrate the impact of the radiation safety limit. First, the natural radioactivity background in dose is of order

$$D_{\mathrm{natural}} \lesssim 0.1\ \mu\mathrm{Sv} \cdot \mathrm{h}^{-1}. \tag{1}$$

For a typical GM counter calibrated with Cs^{137} (662 keV), a dose rate of 0.1 μSv/h corresponds to about 10 counts per minute. This conversion factor is detector dependent, but

Published by the American Physical Society under the terms of the Creative Commons Attribution 4.0 International license. Further distribution of this work must maintain attribution to the author(s) and the published article's title, journal citation, and DOI. Funded by SCOAP³.

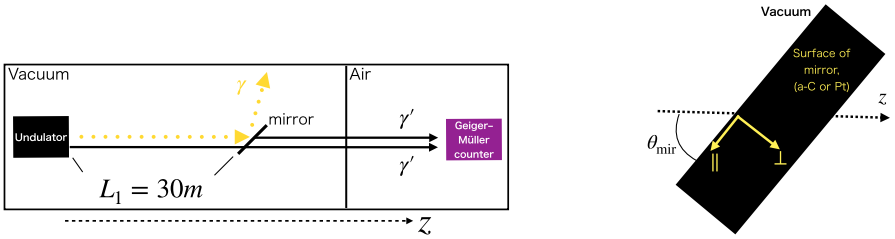


FIG. 1. Schematic view of the setup under consideration (left panel), which reflects a configuration typical of many synchrotron beamlines up to the first optical element. Throughout this Letter I take $L_1 = 30$ m. The mirror is aligned so that most photonlike states are directed into the experimental hutches. A magnified view of the mirror is shown (right panel). The axes relevant for studying the transmission of the dark-photonlike state are indicated.

I adopt it here as a reasonable representative value. Note that the GM counter measures only the photon number flux, while the resulting dose rate is quoted assuming the 662 keV line of Cs^{137}.

As an example, consider an undulator producing photons in the keV range with a photon beam power of 3 kW. The photon production rate can be estimated as

$$\dot{n}_\gamma \sim 10^{21}\ \text{min}^{-1}. \tag{2}$$

In what follows, I neglect the dependence on beamline energy and photon beam power, and adopt this value as a representative choice for this Letter [note that for certain beamlines the power can be as large as $\mathcal{O}(10)$ kW; see, e.g., Ref. [27] where the operation power is 12.3 kW for the SPring-8 beamline]. Since both the production and detection rates for dark photons scale as χ^2, requiring that the signal does not exceed natural radioactivity background significantly, one obtains the order-of-magnitude estimate,

$$\chi_{\text{limit}}^4 \times 10^{21}/\,\text{min} \sim 10/\,\text{min} \quad \Rightarrow \quad \chi_{\text{limit}} \sim 10^{-5}. \tag{3}$$

This limit is already comparable to existing laboratory bounds, $10^{-5} - 10^{-4}$, obtained using the SPring-8 beamline [3]. The reason is that the available photon flux directly at the undulator is many orders of magnitude larger than that typically accessible inside an experimental hutch, where optical components such as mirrors, filters, and spectrometers strongly reduce the flux (see, e.g., Ref. [28]). For instance, the mirrors in Fig. 1 are used to direct the photon beam into experimental hutches. This configuration is typical of many synchrotron beamlines up to the first mirror, even though additional optical components may be installed downstream. In contrast, I exploit the full primary photon flux generated at the undulator.

Next, I study the constraints from radiation safety beyond the simple order-of-magnitude estimate.

Setup and production from undulator—I assume a minimal dark photon A'_μ with mass m and kinetic mixing χ with the visible photon A_μ. The Lagrangian in addition to the standard model one in the interaction basis is given by

$$\mathcal{L} = -\frac{1}{4}F'_{\mu\nu}F'^{\mu\nu} + \frac{\chi}{2}F_{\mu\nu}F'^{\mu\nu} + \frac{1}{2}m^2A'_\mu A'^\mu. \tag{4}$$

Here $F_{\mu\nu}, F'_{\mu\nu}$ denote the field strength of A_μ, and A'_μ, respectively, and m is the dark photon mass. In the interaction basis, only the visible photon field A_μ couples to the electromagnetic current J^μ of ordinary charged particles with the Lagrangian $-J^\mu A_\mu$. The dark photon A'_μ interacts with matter only through the kinetic mixing term, and can thus be produced when a high-intensity photon flux is available.

An *undulator* is a periodic magnetic structure widely used in synchrotron and free-electron-laser facilities. When a relativistic electron beam traverses an array of alternating-polarity magnets, it follows a sinusoidal trajectory and emits synchrotron radiation. Because the motion is periodic, radiation from successive oscillations interferes constructively, resulting in a highly brilliant, collimated, and quasimonochromatic x-ray beam with a narrow spectral bandwidth.

The undulator is characterized by parameters k, K, ϕ, and κ in the notation of Refs. [12,13]. Here k denotes the undulator wave number, related to the period λ_u by $k = 2\pi/\lambda_u$. The parameter K represents the strength of the electron wiggling, while κ and ϕ encode the undulator geometry.

The number of photons produced per electron traversing the undulator is

$$N_\gamma = \sum_{\epsilon^\pm} \int \frac{d^3\vec{k}_\gamma}{(2\pi)^3} \left| f_\gamma(\vec{k}_\gamma) \right|^2. \tag{5}$$

$\epsilon_\pm$ denotes the two photon polarizations. The photon wave packet $f_\gamma(\vec{k}_\gamma)$, neglecting mixing, follows from standard calculations and is well known (see the Supplemental Material for an estimate [29]) [12,13,30]. I only focus on the fundamental harmonic for f_γ for simplicity.

By neglecting matter effects, I introduce the mass eigenfields $A_\mu^{(1)}$ and $A_\mu^{(2)}$, in which both the kinetic and mass terms are diagonalized. Here $A_\mu^{(1)}$ corresponds to the

massless photonlike field, and $A_\mu^{(2)}$ to the massive dark-photonlike field. In this basis, the electromagnetic current couples as $J^\mu A_\mu \simeq J^\mu\left(A_\mu^{(1)} - \chi A_\mu^{(2)}\right)$, neglecting $\mathcal{O}(\chi^2)$ terms.

When the dark photon mass is negligible, one obtains

$$f^{(1)} \approx f_\gamma, \qquad f^{(2)} \approx -\chi f_\gamma. \tag{6}$$

Importantly [13], $f^{(2)} \to 0$ when $m > m_1 \equiv k\gamma/\sqrt{1+(1+\kappa^2)K^2/2}$. This suppression arises because synchrotron radiation in an undulator can be understood as boosted dipole radiation of the electron. In the electron rest frame, the oscillation frequency is $k\gamma/\sqrt{1+(1+\kappa^2)K^2/2}$, so a dark photon heavier than this value cannot be efficiently produced. For the numerical simulations, I approximate this suppression by multiplying $f^{(2)}$ with a Heaviside step function that enforces the above inequality, which provides a good approximation to the full calculation [13].

Throughout this Letter, I neglect the longitudinal mode, whose production and detection are both suppressed by m^2/ω^2 and is therefore irrelevant in the regime $m \ll \omega$ considered here.

Propagation across the mirror—When an x-ray beam (or a weakly mixed dark-photon-like component) encounters a mirror, the coating layer is not a passive reflector but an *active* optical interface that governs how the fields partition into reflected, transmitted, and converted modes. In grazing-incidence optics, the coating is chosen (e.g., Pt, Rh, Ni or low-Z carbides) to exploit total external reflection below the critical angle, with the complex refractive index $n(\omega) = 1 - \delta(\omega) + i\beta(\omega)$ controlling both dispersion and absorption. The discontinuity of the dielectric response across the vacuum-coating boundary fixes the electromagnetic boundary conditions and thus the Fresnel coefficients, including the well-known critical angle $\theta_c \simeq \sqrt{2\delta}$ for x-rays. Taking account of the complex refractive indices, the system including the dark photon can be easily studied by using the standard optical analysis with the continuity condition in the photon-dark-photon system.

For later convenience, I define (see the right panel of Fig. 1) $\theta_{\rm mir} \equiv (\pi/2) - \arccos(\hat{n}\cdot\hat{e}_z)$, where $\hat{n}$ is the normal vector of the mirror and $\hat{e}_z$ is the unit vector along the z direction (the beam axis). Since the photon (dark photon) beam spread is of order $1/\gamma \lesssim 10^{-4}$ (see Table I), which is smaller than a typical mirror angle $\theta_{\rm mir} \gtrsim 0.1°$, I neglect the angular dependence when estimating the transmission.

From the continuity conditions at the boundary of the mirror (see the Supplemental Material [29]), I obtain the number of massive states that pass through the mirror [32]:

$$N_{\rm mir}^{(2)} \simeq \sum_{\epsilon^\pm} \int \frac{d^3k_{\rm mir}^{(2)}}{(2\pi)^3}|\mathcal{M}|^2, \tag{7}$$

TABLE I. Parameters used in deriving the limits. Here $\omega_{\rm typ} \equiv k\gamma^2/(1+K^2)$ denotes the typical energy of the fundamental harmonic. The factor of 2 is included to indicate the on-axis value, following standard convention. "a-c" denotes amorphous carbon. Here I consider helical undulators, for simplicity, $\kappa = 1$ and $\phi = 0$.

	γ	K	$2\pi/k$ (mm)	$Lk/(2\pi)$	$2\omega_{\rm typ}$ (keV)	Mirror coating	$\theta_{\rm mir}$
①	6000	1	30	33	1.4	a-c	2°
②	16000	1	40	125	8	Pt	0.1°
③	13000	1	20	75	10	Pt	0.1°
④	12000	0.5	20	73	14	Pt	0.1°

$$\mathcal{M} \approx -\frac{k_{\perp,\rm vac}^{(1)}(k_{\perp,\rm mir}^{(1)} + k_{\perp,\rm vac}^{(2)})}{k_{\perp,\rm vac}^{(2)}(k_{\perp,\rm mir}^{(1)} + k_{\perp,\rm vac}^{(1)})}\Delta\chi^{\rm eff}\Theta(m_2 - m)f_\gamma + e^{-i\frac{m^2}{2\omega}L_1}\chi\Theta(m_1 - m)f_\gamma, \tag{8}$$

where I used the wave packets discussed in Eq. (6) to estimate the amplitude $\mathcal{M}$ for dark-photon production. L_1 denotes the distance between the undulator and the mirror, and I have expanded the phase to leading order in m^2. In $\vec{k}_i^{(\alpha)}$, α labels the mass eigenstate and i = vac (vacuum) or mir (mirror material), while $\perp$ denotes the component perpendicular to the mirror surface (see the right panel of Fig. 1). $\Delta\chi^{\rm eff}$ represents the difference between the effective mixing parameters in the mirror and in vacuum, including matter effects (see the Supplemental Material [29]). I assume that the mirror coating is sufficiently thick that the photonlike state at shallow incidence does not penetrate. Accordingly, I include Heaviside step functions to model the kinematic cutoffs: $\Theta(m_1 - m)$ accounts for the suppression of dark-photon production in the undulator, while $\Theta(m_2 - m)$ enforces the requirement that the relevant perpendicular momentum component at the mirror interface is sufficient. Here $m_2 \equiv |\vec{k}_{\perp,\rm mir}^{(2)}| \simeq \sin\theta_{\rm mir}|\vec{k}_{\rm mir}^{(2)}|$.

In general, additional regeneration of photonlike states can occur: when the heavier mass eigenstate propagates through the mirror, it may regenerate lighter mass eigenstates on the other side. Moreover, realistic mirrors often consist of multiple layers, and at each boundary additional dark-photonlike states may be produced. Similar effects can arise in other optical components and even in the shielding. Once produced, a dark-photonlike state experiences only $\mathcal{O}(\chi^2)$-suppressed attenuation in the environment, which can be safely neglected. Additional production beyond the undulator and the first mirror would therefore only enhance the sensitivity. The present analysis, restricted to these contributions, thus provides a conservative estimate.

Novel limits from radiation safety—Once the dark-photonlike states are produced, most of them pass through all optical systems, shielding, and even air. However, due to

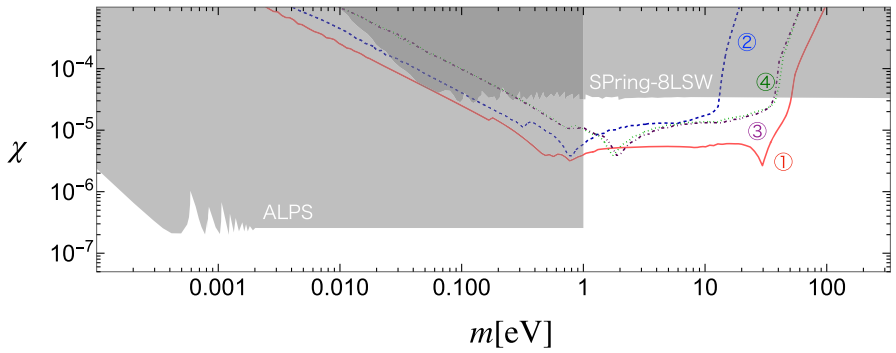


FIG. 2. Limits on the dark photon mixing parameter χ as a function of the dark photon mass m, derived from radiation-safety considerations (red solid, blue dashed, green dotted, and purple dash-dotted lines correspond to ①–④ in Table I, respectively). $L_{\rm det} = 10$ cm is assumed. Existing laboratory limits (ALPS, SPring8-LSW) taken from Refs. [2,3] are shaded in gray. See, e.g., Ref. [38] for more stringent limits on dark photons produced in astrophysical or cosmological environments.

their nonvanishing mixing, there remains a rare probability for them to interact with a "photon detector."

As a concrete example, I consider an argon-filled GM counter (see Ref. [33]). The detector is a metal cylinder of length ∼10 cm and diameter ∼1 cm with a thin (∼50 μm) central anode wire, filled with high-purity Ar gas at ∼1 atm and room temperature. Since the beam spread is of order $1/\gamma \lesssim 10^{-4}$, the counter can cover the entire dark-photon beam if placed within 100 m from the undulator. Incident radiation ionizes Ar, producing primary pairs that trigger Townsend avalanches, with an amplification factor of $\mathcal{O}(10^{8-10})$, ensuring efficient detection. The effective energy response for ordinary photons starts from a few keV due to the opaque ∼5–10 μm entrance window, but dark photons traverse the window essentially without attenuation, retaining sensitivity down to the sub-keV range.

A dark-photonlike state interacts with Ar with effective probability [13,34–36]

$$P_{\rm det}^{\rm eff} = \chi^2 \times \frac{m^4}{|m^2 - \Pi_{\rm Ar}|^2} \times \frac{-\Im\Pi_{\rm Ar}}{2\omega} \times L_{\rm det}, \tag{9}$$

with $L_{\rm det} \approx 10$ cm the effective length of Ar. The factor $(m^4/|m^2 - \Pi_{\rm Ar}|^2)$ suppresses detection at $m^2 \ll |\Pi_{\rm Ar}|$, while $-\Im\Pi_{\rm Ar}/(2\omega)$ is the linear attenuation coefficient. The first ionization energy of Ar is ∼16 eV, so interactions with dark photons of $\gtrsim$ sub-keV energy readily produce $\mathcal{O}(10)$ initial electrons, which then trigger avalanches and yield detectable signals.

Thus I arrive at the final formula for the detection probability per electron traversing the undulator,

$$N_{\rm det} = \sum_{e^\pm} \int \frac{d^3\vec{k}_{\rm mir}^{(2)}}{(2\pi)^3} |\mathcal{M}|^2 \times P_{\rm det}(\vec{k}_{\rm mir}^{(2)}). \tag{10}$$

From this I obtain the effective photon-photon transmission rate, $P_{\gamma\to\gamma}^{\rm eff} \equiv (N_{\rm det}/N_\gamma)$ with N_γ given in Eq. (5). Assuming Eq. (2), the dark-photon signal rate is given by $P_{\gamma\to\gamma}^{\rm eff}\dot{n}_\gamma$, and I set the exclusion limit by requiring

$$P_{\gamma\to\gamma}^{\rm eff}\dot{n}_\gamma < 100\ {\rm min}^{-1}, \tag{11}$$

which corresponds to 1 order of magnitude larger than natural background radiation, at which conventional GM counters typically trigger alerts [37].

The derived limits are shown in Fig. 2 for the parameter sets ①–④ in Table I, chosen to mimic representative beamlines at NanoTerasu, SPring-8, KEK-PF, and ESRF, corresponding to the red solid, blue dashed, green dotted, and purple dash-dotted curves, respectively.

Since some technical details, such as mirror coatings, are not always available in the literature, I adopt conventional choices [For ①, the limit does not change significantly when silicon is used as the mirror coating, since $\Pi_{\rm Si}(\omega) \approx \Pi_{\rm a\text{-}c}(\omega)$ for $\omega \sim$ KeV.]. I also note that there exist much stronger constraints from searches for dark photons produced in astrophysical objects or in the early Universe (see, e.g., Ref. [38]), whereas the laboratory limit discussed here is independent of astrophysical and cosmological model assumptions.

At low masses ($m \lesssim$ eV), the sensitivity loss is mainly due to the suppression of the mixing through repeated Ar interactions. Depending on the energy, a narrow resonance can appear when m is close to the plasma mass [see Eq. (9) and the figure in the Supplemental Material [29]], because at relatively high energies β can be suppressed compared to δ (see the figure in the Supplemental Material [29]).

At higher masses, sensitivity decreases because undulators cease to directly produce dark photons ($m > m_1$), and straight transmission through mirrors is suppressed by the dispersion relation ($m > m_2$). The cutoff m_2 is controlled by the mirror angle $\theta_{\rm mir}$: larger $\theta_{\rm mir}$ allows more momentum modes of f_γ to contribute to $N_{\rm mir}$ and extends the sensitivity to higher masses. For example, with

$\theta_{\rm mir} = 2°$ (amorphous carbon coating), the resonant region related to the plasma mass of carbon can even be reached.

In practice, synchrotron facilities employ a variety of beam lines with different energies and mirror configurations, so the limits presented here should be regarded as representative examples. If radiation-safety monitoring were systematically applied across all beam lines, a much broader set of constraints could be obtained.

For comparison, the most stringent existing laboratory limits [2,3] are also shown (gray shaded region; the data are taken from Ref. [38]). The ALPS experiment employs a near-infrared laser with $\omega \sim 1$ eV as the light source and is therefore kinematically sensitive only to dark photons with masses below 1 eV [2]. The SPring-8 experiment is an LSW search performed inside an experimental hutch using the undulator as the light source [3]. In that configuration, the available photon flux is significantly reduced relative to the present setup, which utilizes the full primary photon flux generated at the undulator. The limits derived here surpass the existing laboratory bounds in the mass range $m = 1$–50 eV. This highlights the potential impact of a "parasitic experiment" at synchrotron radiation facilities; a more sophisticated detector would further improve the sensitivity.

Acknowledgments—W. Y. is thankful for the useful discussions with Junya Yoshida and Toshio Namba. This work is supported by JSPS KAKENHI Grants No. 22K14029 and No. 23K22486 and the Tokyo Metropolitan University Grant for Young Researchers (Selective Research Fund).

Data availability—The data that support the findings of this article are not publicly available. The data are available from the authors upon reasonable request.

[1] J. Redondo and A. Ringwald, Contemp. Phys. **52**, 211 (2011).
[2] K. Ehret *et al.*, Phys. Lett. B **689**, 149 (2010).
[3] T. Inada, T. Namba, S. Asai, T. Kobayashi, Y. Tanaka, K. Tamasaku, K. Sawada, and T. Ishikawa, Phys. Lett. B **722**, 301 (2013).
[4] M. Betz, F. Caspers, M. Gasior, M. Thumm, and S. W. Rieger, Phys. Rev. D **88**, 075014 (2013).
[5] J. W. D. Halliday *et al.*, Phys. Rev. Lett. **134**, 055001 (2025).
[6] R. Battesti, M. Fouche, C. Detlefs, T. Roth, P. Berceau, F. Duc, P. Frings, G. L. J. A. Rikken, and C. Rizzo, Phys. Rev. Lett. **105**, 250405 (2010).
[7] F. Della Valle, A. Ejlli, U. Gastaldi, G. Messineo, E. Milotti, R. Pengo, G. Ruoso, and G. Zavattini, Eur. Phys. J. C **76**, 24 (2016).
[8] T. Inada *et al.*, Phys. Rev. Lett. **118**, 071803 (2017).
[9] R. Ballou *et al.* (OSQAR Collaboration), Phys. Rev. D **92**, 092002 (2015).
[10] P. Sikivie, D. B. Tanner, and K. van Bibber, Phys. Rev. Lett. **98**, 172002 (2007).
[11] P. Carenza, T. Ferreira, and T. T. Q. Nguyen, arXiv:2507.08932.
[12] W. Yin and J. Yoshida, Phys. Rev. D **111**, 036020 (2025).
[13] W. Yin, arXiv:2507.22055.
[14] See also various models and searches that motivate dark photons in this mass range for dark matter production [15–22] and for addressing the Hubble tension [23]. In particular, several dark matter production mechanisms point to this mass window [18,19], given that the matter-radiation equality occurs around the eV temperature scale, similar to the prediction of the hot dark matter paradigm. See also proposals for dark matter decay searches in this mass range [24,25]. For dark matter searches, one can consider $\gamma' \to \gamma\phi$ with ϕ being a light scalar field, producing a narrow line. Furthermore, multilaser collision experiments may probe dark photons in this mass range via the $\gamma'\gamma\gamma\gamma$ coupling, similar to the ALP search proposed in Ref. [26].
[15] T. Moroi and W. Yin, J. High Energy Phys. 03 (2021) 301.
[16] T. Moroi and W. Yin, J. High Energy Phys. 03 (2021) 296.
[17] K. Nakayama and W. Yin, J. High Energy Phys. 10 (2021) 026.
[18] W. Yin, J. High Energy Phys. 05 (2023) 180.
[19] K. Sakurai and W. Yin, J. High Energy Phys. 03 (2025) 202.
[20] T. Fujita, K. Murai, K. Nakayama, and W. Yin, J. Cosmol. Astropart. Phys. 04 (2024) 007.
[21] N. Kitajima and K. Nakayama, J. Cosmol. Astropart. Phys. 07 (2023) 014.
[22] P. W. Graham, J. Mardon, and S. Rajendran, Phys. Rev. D **93**, 103520 (2016).
[23] S. Nakagawa, F. Takahashi, and W. Yin, Phys. Rev. D **107**, 063016 (2023).
[24] T. Bessho, Y. Ikeda, and W. Yin, Phys. Rev. D **106**, 095025 (2022).
[25] T. Bessho, Y. Ikeda, and W. Yin, Proc. SPIE Int. Soc. Opt. Eng. **13096**, 1309678 (2024).
[26] A. Nobuhiro, Y. Hirahara, K. Homma, Y. Kirita, T. Ozaki, Y. Nakamiya, M. Hashida, S. Inoue, and S. Sakabe, Prog. Theor. Exp. Phys. **2020**, 073C01 (2020).
[27] T. Mochizuki, Y. Sakurai, D. Shu, T. Kuzay, and H. Kitamura, Synchrotron Radiat. News **5**, 1199 (1998).
[28] https://beamline.harima.riken.jp/en/bl_info/bl43lxu_info_en.html.
[29] See Supplemental Material at http://link.aps.org/supplemental/10.1103/snnn-wqxg for reviews of the derivations of photon production in an undulator and of the continuity conditions at material boundaries in the photon–dark photon system, which includes Refs. [12,13,30,31].
[30] J. D. Jackson, *Classical Electrodynamics* (John Wiley & Sons, New York, 1998).
[31] B. L. Henke, E. M. Gullikson, and J. C. Davis, At. Data Nucl. Data Tables **54**, 181 (1993).
[32] One can easily see that $|\mathcal{M}|^2$ with small m reduces to the usual oscillation form multiplied by the wave packet when I take $\chi^{\rm eff}_{\rm mir} = 0$, corresponding to $\mathrm{Im}\,\Pi_{\rm mir} \gg m^2$, i.e. when the mirror effectively acts as a perfect "wall."

[33] G. Knoll, Radiation Detection and Measurement (4th ed.) (John Wiley, Hoboken, NJ, 2010).
[34] H. An, M. Pospelov, and J. Pradler, Phys. Rev. Lett. **111**, 041302 (2013).
[35] H. An, M. Pospelov, J. Pradler, and A. Ritz, Phys. Lett. B **747**, 331 (2015).
[36] K. Sakurai and W. Yin, Eur. Phys. J. C **83**, 498 (2023).
[37] See also https://www-pub.iaea.org/MTCD/Publications/PDF/EPR-First_Res-PDA/html/ti5.htm. The threshold 1 μSv/h is larger than the actual radiation-safety level adopted in facilities, and thus provides a conservative limit.
[38] A. Caputo, A. J. Millar, C. A. J. O'Hare, and E. Vitagliano, Phys. Rev. D **104**, 095029 (2021).